

ALMA will determine the spectroscopic redshift $z > 8$ with FIR [O III] emission lines

A. K. Inoue¹, I. Shimizu^{1,2}, Y. Tamura³, H. Matsuo⁴, T. Okamoto⁵, and N. Yoshida^{6,7}

akinoue@las.osaka-sandai.ac.jp

Received _____; accepted _____

¹College of General Education, Osaka Sangyo University, 3-1-1 Nakagaito, Daito, Osaka 574-8530, Japan

²Department of Astronomy, The University of Tokyo, 7-3-1 Hongo, Tokyo 113-0033, Japan

³Institute of Astronomy, The University of Tokyo, Mitaka, Tokyo 181-0015, Japan

⁴National Astronomical Observatory of Japan, 2-21-1 Osawa, Mitaka, Tokyo 181-8588, Japan

⁵Department of CosmoSciences, Graduate School of Science, Hokkaido University, N10 W8, Kitaku, Sapporo 060-0810, Japan

⁶Department of Physics, The University of Tokyo, 7-3-1 Hongo, Tokyo 113-0033, Japan

⁷Kavli Institute for the Physics and Mathematics of the Universe, TODIAS, The University of Tokyo, 5-1-5 Kashiwanoha, Kashiwa, Chiba 277-8583, Japan

ABSTRACT

We investigate the potential use of nebular emission lines in the rest-frame far-infrared (FIR) for determining spectroscopic redshift of $z > 8$ galaxies with the Atacama Large Millimeter/sub-millimeter Array (ALMA). After making a line emissivity model as a function of metallicity, especially for the [O III] 88 μm line which is likely to be the strongest FIR line from H II regions, we predict the line fluxes from high- z galaxies based on a cosmological hydrodynamics simulation of galaxy formation. Since the metallicity of galaxies reaches at $\sim 0.2 Z_{\odot}$ even at $z > 8$ in our simulation, we expect the [O III] 88 μm line as strong as 1.3 mJy for 27 AB objects, which is detectable at a high significance by < 1 hour integration with ALMA. Therefore, the [O III] 88 μm line would be the best tool to confirm the spectroscopic redshifts beyond $z = 8$.

Subject headings: cosmology: observations — galaxies: evolution — galaxies: high-redshift

1. Introduction

Finding the highest redshift objects is placing constraints on the theory of baryonic physics to form luminous objects in the Universe. The latest survey with the Hubble Space Telescope (HST) has provided a number of candidates of $z > 7$ galaxies by the so-called drop-out technique (e.g., Ellis et al. 2013). However, the redshifts of these Lyman break galaxies (LBGs) are not yet confirmed through spectroscopy. Since the rest-frame ultraviolet (UV) continuum of the LBGs are too faint (> 27 AB) to be detected with current spectrograph, it was often assumed that Ly α emission is the best tool to confirm the redshift. Yet, attempts to detect Ly α for $z > 8$ LBGs failed (Brammer et al. 2013; Bunker et al. 2013; Capak et al. 2013; Treu et al. 2013), indicating that Ly α was substantially weakened by the intergalactic neutral hydrogen before the completion of the cosmic reionization. Otherwise the LBGs were just interlopers (Pirzkal et al. 2013; Brammer et al. 2013). If Ly α emission at $z > 8$ is so weakened that we cannot detect, we should consider other emission lines to confirm their redshift.

Considering the superb ability of the Atacama Large Millimeter/sub-millimeter Array (ALMA), the rest-frame far-infrared (FIR) emission lines may be attractive. For example, the [C II] 158 μm line is very luminous and often detected from high- z sources including $z > 6$ QSOs (Maiolino et al. 2005). However, the line is not detected from $z > 6$ Ly α emitters (Walter et al. 2012; Kaneker et al. 2013; Ouchi et al. 2013), suggesting a different situation of the interstellar medium in these high- z low-metallicity galaxies. In addition, the [C II] line at $8.0 < z < 10.6$, where the highest- z LBGs reside, is redshifted into the ALMA band 5 not available soon.

The FIR [O III] lines at 52 and 88 μm are known as prominent lines from H II regions since 1970s (Ward et al. 1975), while the lines have been rarely discussed in the high- z context so far because of the lack of suitable instruments. The first FIR [O III] detection

from cosmologically distant sources is reported by Ferkinhoff et al. (2010) from two $z \simeq 3$ and 4 gravitationally lensed dusty AGN/starburst galaxies. In the local Universe, the Infrared Space Observatory (ISO) and the Japanese Infrared Satellite AKARI detected the lines from Galactic H II regions (Mizutani et al. 2002; Matsuo et al. 2009), from a giant H II region, 30 Doradus, in the Large Magellanic Cloud (LMC) (Kawada et al. 2011), and from many nearby galaxies (Brauer et al. 2008). Interestingly, recent *Herschel* observations have revealed that the [O III] 88 μm line is often stronger than the [C II] line in low-metallicity nearby dwarf galaxies (Figure 5 of Madden et al. 2012; see also Cormier et al. 2012), suggesting the usefulness of the [O III] line at high- z where most galaxies are low-metallicity. Last but not least, the [O III] 88 μm line at $8.1 < z < 11.3$ falls into the ALMA band 7 in operation.

In section 2, we construct a FIR nebular emission model in high- z Universe based on our cosmological simulation and the photoionization code CLOUDY, followed by the expected FIR line fluxes presented in section 3. Finally, we discuss the feasibility for detecting the lines from $z > 8$ galaxies with ALMA in section 4.

Throughout this Letter, we adopt a Λ CDM cosmology with the matter density $\Omega_{\text{M}} = 0.27$, the cosmological constant $\Omega_{\Lambda} = 0.73$, the Hubble constant $h = 0.7$ in the unit of $H_0 = 100 \text{ km s}^{-1} \text{ Mpc}^{-1}$ and the baryon density $\Omega_{\text{B}} = 0.046$. The matter density fluctuations are normalized by setting $\sigma_8 = 0.81$ (Komatsu et al. 2011). All magnitudes are quoted in the AB system (Oke 1990).

2. Model of FIR H II region lines in high- z

In this Letter, we consider only lines from H II regions, and then, we assume the line luminosity, L_{line} , to be proportional to the instantaneous star formation rate (SFR) of a

galaxy, \dot{M}_* ;

$$L_{\text{line}} = C_{\text{line}}(Z, U, n_{\text{H}})\dot{M}_*, \quad (1)$$

where C_{line} is the line emissivity per unit SFR and depends on the metallicity, Z , the ionization parameter, U , and the hydrogen number density, n_{H} , in H II regions of the galaxy. This assumption is usual for hydrogen recombination lines because the Lyman continuum (LyC) making H II regions are emitted only by massive stars whose life-time (~ 1 Myr) is short enough to represent the instantaneous SFR of galaxies (e.g., Kennicutt 1998). Given that the same LyC also ionizes the metal atoms, the similar assumption for metal forbidden lines as equation (1) would be reasonable. However, the proportional factor, C_{line} , depends on the nebular parameters of U and n_{H} as well as the metallicity Z for the case of forbidden lines. On the other hand, we avoid modelling photodissociation regions and molecular clouds surrounding H II regions because it requires more complex physical and chemical processes (e.g., Abel et al. 2005; Nagao et al. 2011) and may cause a large uncertainty, although it enables us to predict some strong FIR lines such as [C II] 158 μm and [O I] 63 μm . It would be an interesting future work.

Using the photoionization code CLOUDY version c13.01 (Ferland et al. 2013), we make a model of C_{line} . The CLOUDY calculations are similar to Inoue (2011). We assume six metallicities as $\log_{10}(Z/Z_{\odot}) = -5.3, -3.3, -1.7, -0.7, -0.4,$ and 0.0 , three ionization parameters as $\log_{10} U = -3.0, -2.0,$ and -1.0 , and four hydrogen number densities as $\log_{10}(n_{\text{H}}/\text{cm}^{-3}) = 0.0, 1.0, 2.0,$ and 3.0 . The ‘‘H II region’’ set of the gas elemental abundance based on the observations of the Orion nebula is used and the ‘‘Orion type’’ dust grains are included. The nebular and stellar metallicities are assumed to be equal. The shape of the stellar spectra are taken from STARBURST99 (Leitherer et al. 1999) and Schaerer (2002), depending on the metallicity. The initial mass function (IMF) is assumed to be a Salpeter one with $0.1\text{--}100 M_{\odot}$. We consider the scenario of a constant star formation of 10 Myr but the age of the star formation has negligible impact on C_{line} . We

also note that negligible differences are found when we adopt another population synthesis code PÉGASE ver. 2 (Fioc & Rocca-Volmerange 1997). We also assume a constant density throughout the H II regions and the plain-parallel geometry. The calculations are stopped if the electron temperature becomes less than $10^{3.5}$ K or the electron fraction becomes less than 1%. No escape of the LyC from H II regions (and galaxies) is considered. The line emissivities are reduced approximately by a factor of $1 - f_{\text{esc}}$ when the escape fraction is f_{esc} .

From the CLOUDY calculations, we find that the [O III] 88 μm line is the strongest line for the nebular parameters examined in this Letter. Figure 1 shows the [O III] line luminosities per unit SFR as a function of metallicity for 9 combinations of nebular parameters as indicated in the panel. The luminosities with $\log_{10}(n_{\text{H}}/\text{cm}^{-3}) = 3.0$ are much smaller than those shown in Figure 1 as a trend found in the figure: a smaller emissivity for a higher density. The line emissivities for a constant ionization parameter are roughly proportional to the metallicity when $Z < 0.1Z_{\odot}$ as the oxygen abundance increases. When $Z > 0.1Z_{\odot}$, the dependence becomes weaker because of lower LyC emissivity for higher metallicity.

For a comparison, we plot observational estimates in Figure 1. Kawada et al. (2011) reported the flux ratio of $F_{[\text{OIII}]88}/F_{\text{H}\alpha} \simeq 0.5$ to 1.0 in 30 Doradus of the LMC. Adopting the conversion formula from H α luminosity to SFR by Hirashita et al. (2003), we obtain the emissivity shown by the diamond.¹ The vertical error-bar indicates the uncertainty of the conversion and the sample variance of the flux ratio. The

¹In the formula of Hirashita et al. (2003), there are two parameters: the dust correction factor for H α ($A_{\text{H}\alpha}$) and the hydrogen ionizing fraction in the LyC (f). Note that a part of the Lyman continuum is absorbed by dust before using hydrogen ionization (Inoue et al. 2001). We take $A_{\text{H}\alpha} = 0.5$ and $f = 0.7$ for the LMC from Inoue (2001).

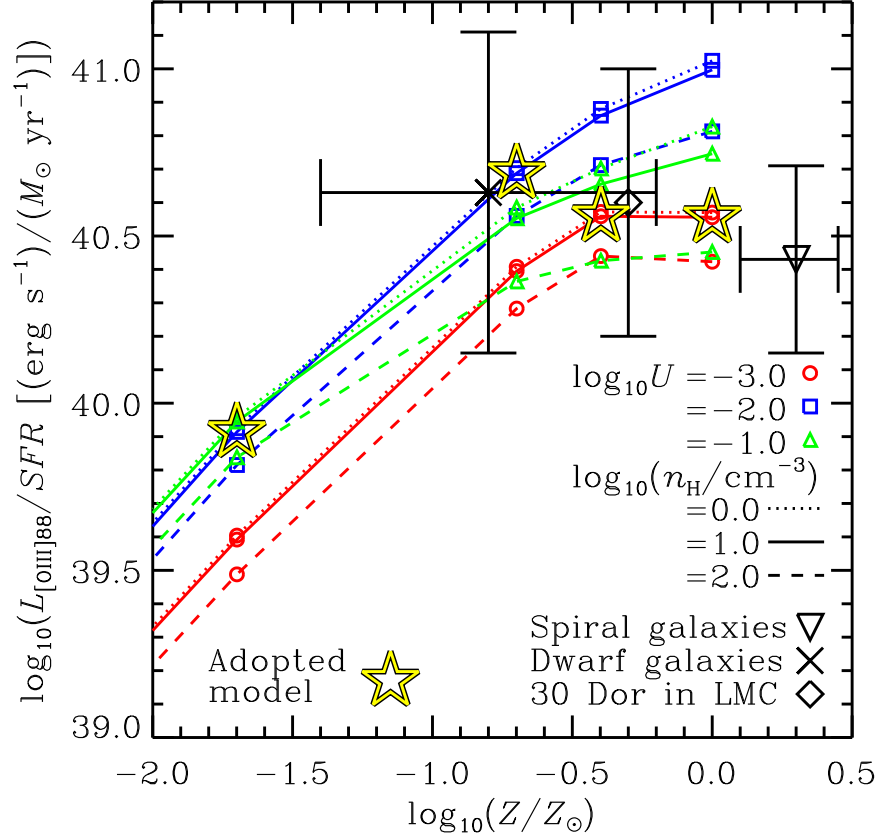


Fig. 1.— Luminosities of the [O III] 88 μm line per unit star formation rate (a Salpeter initial mass function with 0.1–100 M_{\odot}) as a function of metallicity for 9 combinations of the ionization parameter $\log_{10} U$ and the hydrogen density $\log_{10} n_{\text{H}}$ indicated in the panel. No escape of the Lyman continuum from H II regions is taken into account. The inverse triangle, cross, and diamond with error-bars are observational estimates of nearby spiral galaxies (Brauer et al. 2008), nearby dwarf galaxies (Madden et al. 2012, 2013), and 30 Doradus in the Large Magellanic Cloud (Kawada et al. 2011), respectively. The large five-pointed stars indicate the models adopted in this Letter and summarized in Table 1.

metallicity is taken from van den Bergh (2000). Madden et al. (2012, 2013) reported $\log_{10}(F_{[\text{O III}]88}/F_{\text{FIR}}) = -2.04 \pm 0.29$ for nearby low-metallicity dwarf galaxies. Converting the FIR luminosity to SFR by using the formula of Hirashita et al. (2003), we obtain the cross point with error-bars.² The vertical error-bar includes the uncertainty of the conversion and the observed sample variance. The horizontal error-bar indicates the sample metallicity distribution taken from Madden et al. (2013). Brauher et al. (2008) presented a compilation of [O III] 88 μm observations of nearby galaxies. If we select only spiral galaxies from their sample, we obtain $\log_{10}(F_{[\text{O III}]88}/F_{\text{FIR}}) = -2.61 \pm 0.20$. Again adopting the formula by Hirashita et al. (2003), we obtain the inverse triangle with error-bars.³ The vertical error-bar includes the uncertainty of the conversion and the sample variance. The metallicity is estimated from the mean absolute magnitude of the sample galaxies via the correlation between the magnitude and the metallicity presented by Tremonti et al. (2004).

While the uncertainties are still large, we may find a trend that the [O III] emissivity is slowly decreases as the metallicity increases from $\approx 0.2Z_{\odot}$. We also find that no single combination of the nebular parameters of $\log_{10} U$ and $\log_{10} n_{\text{H}}$ reproduces this trend. Then, we consider a model with a constant $\log_{10} n_{\text{H}}$ but a higher $\log_{10} U$ at lower metallicities. Such a trend may be realized by a higher LyC production rate and a harder spectrum of

²First, we converted the FIR (40–120 μm) luminosity estimated from IRAS measurements to the total IR (8–1000 μm) luminosity, assuming the dust temperature of 30 K and the IR emissivity index of 1.0. Then, the IR luminosity is converted to the SFR by the formula of Hirashita et al. (2003) (see also Inoue et al. 2000) which has three parameters. We adopt $f = 0.8 \pm 0.2$, $\epsilon = 0.3 \pm 0.2$ and $\eta = 0.1 \pm 0.1$ for low-metallicity starbursting galaxies.

³The FIR to IR conversion is done with the dust temperature of 30 K and the emissivity index of 1.0. The IR to SFR conversion is done with the recommended factor for nearby star-forming galaxies in Hirashita et al. (2003).

lower metallicity stars. We therefore adopt the models indicated by the large five-pointed stars in this Letter. However, we should note that this may not be a unique combination of the parameters compatible with the observations. Table 1 is a summary of C_{line} for 11 H II region lines calculated in the adopted models.

In order to predict the FIR line fluxes from high- z galaxies, we need their SFRs in equation (1). We adopt a cosmological simulation by Shimizu et al. (2013) which was developed to examine physical properties of LBGs at $z \sim 7\text{--}10$. The simulation code is based on a Tree-PM smoothed particle hydrodynamics code GADGET-3 updated from GADGET-2 (Springel 2005). We have implemented star formation, supernova (SN) feedback and chemical enrichment following Okamoto et al. (2008); Okamoto & Frenk (2009); Okamoto et al. (2010). We employ $N = 2 \times 640^3$ particles for dark matter and gas in a comoving volume of $50h^{-1}$ Mpc cube. The mass of a dark matter particle is $3.01 \times 10^7 h^{-1} M_{\odot}$ and that of a gas particle is initially $6.09 \times 10^6 h^{-1} M_{\odot}$. Gas particles can spawn star particles when they satisfies a set of criteria for star formation. In each snapshot of the simulation, we run the SUBFIND algorithm (Springel et al. 2001) to identify groups of dark matter, gas, and star particles as galaxies. Parameters in the code such as SN feedback and dust attenuation are calibrated so as to reproduce the stellar mass functions and UV luminosity functions observed at $z \geq 7$. We have constructed a light-cone output from a number of snapshots of the simulation, calculated the apparent magnitudes in a number of broadband filters, and then, applied the exactly same color selection criteria as real observations to select LBGs at $z \sim 7, 8, 9$, and 10. See Shimizu et al. (2013) for more details.

The FIR line fluxes, $F_{\text{line}s}$, for individual galaxies extracted from the cosmological simulation are estimated by the following procedure; First, we assign $C_{\text{line}}(Z_{\text{neb}})$ s to each

simulated LBG, where Z_{neb} is the “nebular” metallicity⁴ of the LBG, by interpolating the values in Table 1. Then, we obtain the line luminosities by equation (1) with the SFR of the simulated LBG. Finally, the luminosities are converted to the fluxes by the luminosity distance in the light-cone. In addition, the peak intensities of the lines, $F_{\nu_0}^{\text{peak}}$, are calculated by the following formula: $F_{\nu_0}^{\text{peak}} = F_{\text{line}}(1+z)c/\nu_0/v_{1D}/\sqrt{\pi}$, where c is the light speed, z is the redshift, ν_0 is the rest-frame line center frequency, and v_{1D} is the standard deviation of the one-dimensional gas velocity which is assumed to be equal to that of the dark matter.

3. Expected FIR line fluxes of high- z galaxies

Figure 2 shows the expected flux of the [O III] 88 μm line, which is the strongest among the lines examined in this Letter, from the simulated LBGs at $z \sim 7$ to 10 as a function of the apparent magnitudes. We find that a good correlation between the line flux and the apparent rest-frame UV magnitude and it does not change along the redshift very much. The dispersion is larger for fainter galaxies because the dispersions of metallicity, SFR, and dust attenuation are also larger for fainter galaxies in our simulation since the SN feedback affects them largely and their star formation histories fluctuate more (Shimizu et al. 2013).

Relating the SFR in equation (1) to the UV magnitude, we can derive an analytic relation between the line flux and the apparent UV magnitude:

$$\begin{aligned} \log_{10} F_{\text{line}} = & -0.4(m_{\text{UV}} - A_{\text{UV}} + AB_0) + \log_{10} C_{\text{line}} \\ & - \log_{10} C_{\text{UV}} + \log_{10}(1 - f_{\text{esc}}) - \log_{10}(1 + z), \end{aligned} \quad (2)$$

where F_{line} is the line flux in cgs unit, m_{UV} is the apparent UV magnitude in the AB system, A_{UV} is the UV dust attenuation, $AB_0 = 48.6$ is the zero point of the AB

⁴A weighted mean metallicity of star particles composing of a galaxy with the LyC luminosity of the particles as the weight (Shimizu et al. 2013).

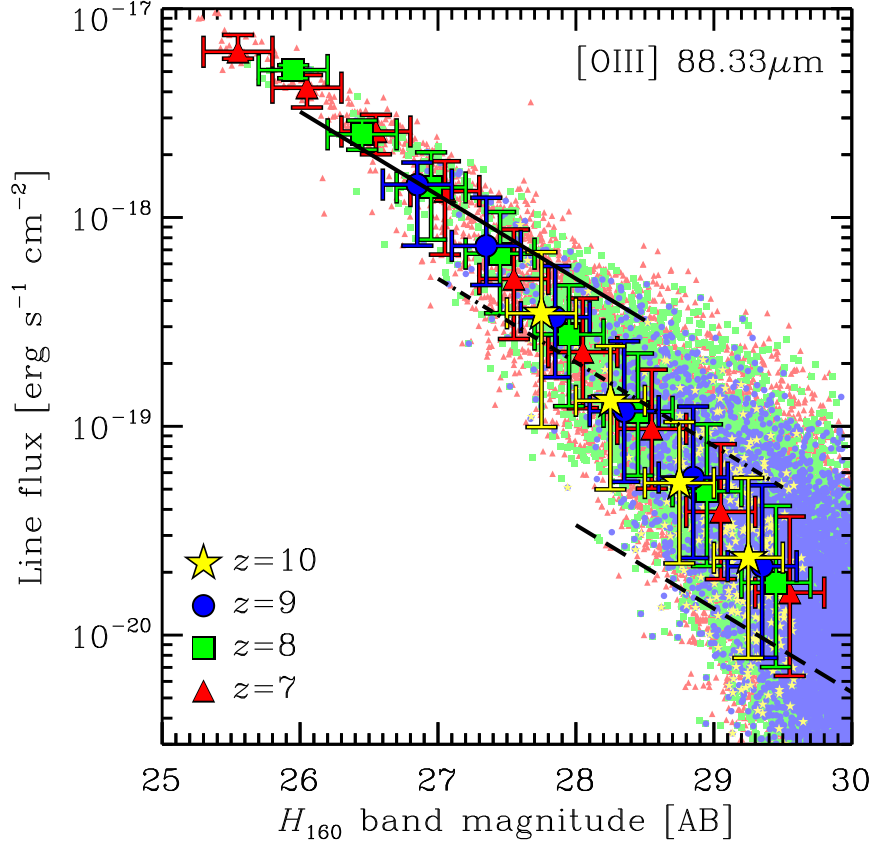


Fig. 2.— The expected line flux of the [O III] 88 μm line from Lyman break galaxies at $z \sim 7$ (triangles), 8 (squares), 9 (circles), and 10 (stars) in the simulation of Shimizu et al. (2013). The horizontal axis is the simulated apparent HST/WFC3 H_{160} magnitude. The large symbols with error-bars show the median values and the central 68% ranges for the galaxies divided into 0.5 magnitude step bins shown by the horizontal error-bars. The solid, dot-dashed, and dashed lines show the equation (2) for $z = 7$, $f_{\text{esc}} = 0$, and a set of $(Z/Z_{\odot}, A_{\text{UV}}) = (0.2, 1.0)$, $(0.2, 0.0)$, and $(0.02, 0.0)$, respectively.

system in cgs unit, f_{esc} is the LyC escape fraction, z is the redshift, C_{line} is the line emissivity in Table 1, and C_{UV} is the ratio of the UV luminosity-to-the SFR. For > 100 Myr constant SFR and the Salpeter IMF in §2, we obtain the almost constant value of $\log_{10}(C_{\text{UV}}[\text{erg s}^{-1}/(M_{\odot} \text{ yr}^{-1})]) = 27.84$ at the rest-frame 2000 Å for $Z/Z_{\odot} = 0.02$ to 1.0. In Figure 2, we show 3 cases of the analytic relations. The metallicity and attenuation values are taken from the results of Shimizu et al. (2013). From this comparison, the readers may confirm that the galaxies are already enriched to $Z_{\text{neb}} = 0.01\text{--}0.5Z_{\odot}$ and typically $\sim 0.2Z_{\odot}$ at these high- z .

In Figure 3, we show the expected peak flux density of the [O III] 88 μm line as a function of the apparent magnitude. The one-dimensional velocity dispersion of the dark matter particles composing the simulated LBGs is 42 ± 4 (or 26 ± 3) km s^{-1} for $H_{160} = 27$ (28.5). This is somewhat smaller than those of optical [O III] lines measured in $z \sim 3$ LBGs (e.g., Pettini et al. 1998). However it is reasonable given a lower mass of the $z \geq 7$ LBGs as Shimizu et al. (2013) expect $< 10^{11} M_{\odot}$ for $H_{160} > 27$. We expect 1.3 ± 0.5 (or 0.2 ± 0.1) mJy for $H_{160} = 27$ (28.5) objects.⁵ If the readers require to estimate the strengths of other emission lines, they can do by a scaling with the numbers in Table 1.

4. Follow-up feasibility with ALMA

Let us consider observing the [O III] 88 μm line with ALMA. In the band 7 (275–373 GHz), we can capture the line from $8.1 \leq z \leq 11.3$ where the current highest- z LBGs

⁵Other physical parameters of the simulated galaxies are as follows: SFR of 20 ± 7 (3.0 ± 1.5) $M_{\odot} \text{ yr}^{-1}$, “nebular” metallicity of 0.19 ± 0.07 (0.10 ± 0.05) Z_{\odot} , halo mass of $(1.6 \pm 0.3) \times 10^{11}$ ($(4.5 \pm 1.1) \times 10^{10}$) M_{\odot} , and stellar mass of $(2.8 \pm 1.1) \times 10^9$ ($(4.8 \pm 2.4) \times 10^8$) M_{\odot} for $H_{160} = 27$ (or 28.5) AB.

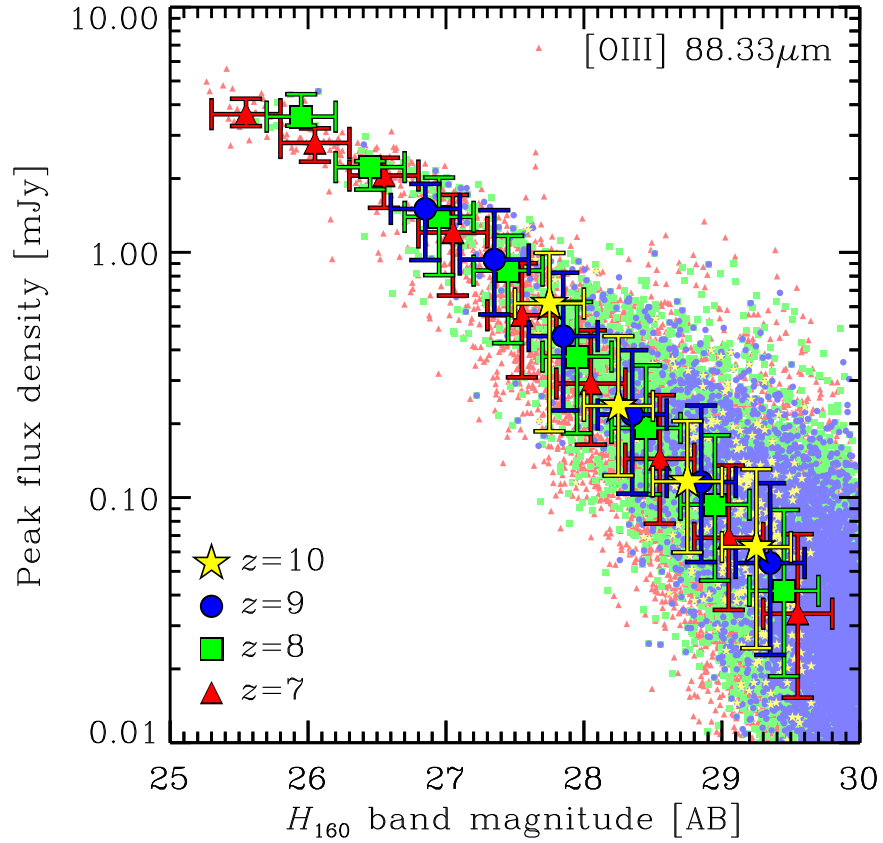


Fig. 3.— The expected peak flux density of the [O III] 88 μm line of Lyman break galaxies at $z \sim 7$ (triangles), 8 (squares), 9 (circles), and 10 (stars) in the simulation of Shimizu et al. (2013). The large symbols with error-bars show the median values and the central 68% ranges.

reside. Using the ALMA Sensitivity Calculator for the Cycle 2, in which we have assumed 50 antennas (full operation), dual polarization, 30 km s^{-1} velocity resolution, declination of $+22^{\text{d}}25'$ (the $z = 9.6$ object by Zheng et al. 2012), and ‘Automatic Choice’ for weather conditions⁶, we obtain the expected sensitivities in Figure 4. We find that the 1.3 mJy [O III] line from a $H_{160} = 27$ object at $8.3 < z < 9.3$ or $9.6 < z < 11.5$ can be detectable at a $> 4\text{-}\sigma$ significance with about 1 hour integration. Since there is a rather strong atmospheric water absorption, we cannot easily detect the line from $9.3 < z < 9.6$. In fact, $H_{160} = 27$ is very bright for LBGs at $z > 8$ but there are some objects found in the recent survey (e.g., Trenti et al. 2011; Oesch et al. 2013). Gravitationally lensed objects are also good targets. Zheng et al. (2012) reported an object with the photometric redshift $z = 9.6$. This object is as bright as $H_{160} = 25.7$ apparently but should be 28.6 without magnification. According to Figure 3, we find the intrinsic and lensed line flux densities of this object are about 0.2 and 3 mJy, respectively. Therefore, we can detect the [O III] line at $> 5\text{-}\sigma$ from this object with only 15 minutes integration.

It is a caveat that we do not know exact redshift prior to the detection. So, we have to scan a range of frequency where a possible line exists. After ALMA Cycle 2, we can use the ‘Spectral Scan’ mode which enables us to cover about 30 GHz by 5 tunings. This corresponds to about $\Delta z \simeq 1$ for the [O III] line at $z \simeq 9$. This is wide enough to probe the redshift range expected by photometry. Another caveat is that we have only a single line even if we detect. Thus, we have to rely on a photometric redshift method to conclude the detected line to be the [O III] $88 \mu\text{m}$ line. Fortunately, we can go to detect other weaker lines such as [O III] $52 \mu\text{m}$ and [N III] $57 \mu\text{m}$ as well as [O I] $63 \mu\text{m}$ and [C II] $158 \mu\text{m}$

⁶The precipitable water vapor is automatically selected depending on the frequency by the Observing Tool for Cycle 2 as shown in the lower panel of Figure 4. This is the default setting and is related to the real operation of the observatory.

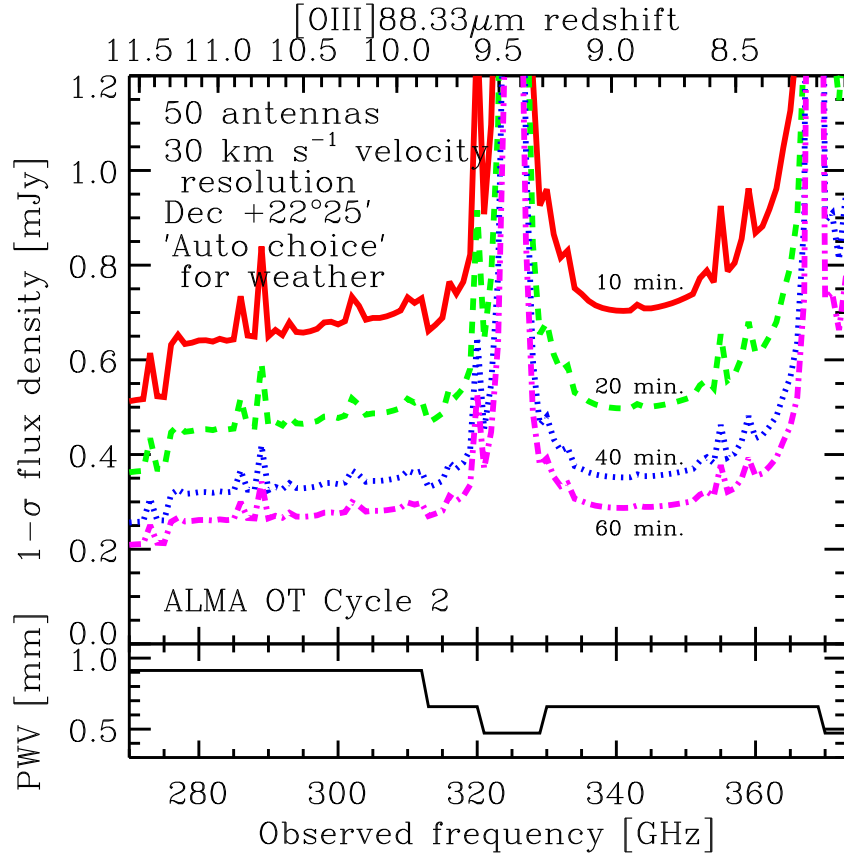


Fig. 4.— The expected ALMA sensitivities in the band 7 with a 10 (solid), 20 (dashed), 40 (dotted), and 60 (dot-dashed) minutes integration under the condition described in the panel. The lower panel shows the precipitable water vapor (PWV) values chosen by the ALMA Observing Tool ‘Automatic Choice’.

because we already know the exact redshift and can invest much time for one integration. The ratios of these FIR lines are very useful for diagnostics of the chemical evolution and ionizing sources in highest- z galaxies.

We thank to Tohru Nagao for useful comments on CLOUDY calculations and Erik Zackrisson for discussions. We acknowledge the financial support of Grant-in-Aid for Young Scientists (A: 23684010; S: 20674003; B: 24740112) by MEXT, Japan. This work is also supported by the FIRST program SuMIRe by the Council for Science and Technology Policy.

Table 1. Line emissivities per unit star formation rate C_{line} in equation (1) adopted in this Letter. The tabulated values are $\log_{10}(C_{\text{line}}[\text{erg s}^{-1}/(M_{\odot} \text{ yr}^{-1})])$. Density is always assumed to be $\log_{10}(n_{\text{H}}/\text{cm}^{-3}) = 1.0$.

Z/Z_{\odot}	$\log_{10} U$	[S IV]	[Ne II]	[Ne III]	[S III]	[S III]	[Ne III]	[O III]	[N III]	[O III]	[N II]	[N II]
		10.51	12.81	15.55	18.67	33.47	36.01	51.80	57.21	88.33	121.7	205.4
1.0	−3.0	38.87	40.01	40.00	40.32	40.72	38.95	40.32	40.14	40.56	39.81	39.82
0.4	−3.0	39.09	39.50	40.07	40.10	40.46	39.02	40.33	39.70	40.56	39.04	39.07
0.2	−2.0	40.12	38.38	40.02	39.86	40.20	38.97	40.46	39.52	40.69	37.67	37.72
0.02	−2.0	39.39	37.43	39.25	39.05	39.36	38.20	39.69	38.74	39.91	36.79	36.85
5×10^{-4}	−2.0	38.07	35.58	37.75	37.42	37.73	36.71	38.18	37.14	38.41	35.25	35.31
5×10^{-6}	−2.0	36.22	33.60	35.85	35.47	35.78	34.81	36.29	35.19	36.52	33.36	33.42

REFERENCES

- Abel, N. P., Ferland, G. J., Shaw, G., & van Hoof, P. A. M., 2005, *ApJS*, 161, 65
- Brammer, G. B., et al., 2013, *ApJ*, 765, L2
- Brauher, J. R., Dale, D. A., Helou, G., 2008, *ApJS*, 178, 280
- Bunker, A. J., et al., 2013, *MNRAS*, 430, 3314
- Capak, P. L., Faisst, A., Vieira, J. D., Tacchella, S., Carollo, M., & Scoville, N. Z. 2013, *ApJ*, in press (arXiv:1307.4089)
- Cormier, D., et al., 2012, *A&A*, 548, 20
- Ellis, R. S., et al., 2013, *ApJ*, 763, L7
- Ferkinhoff, C., Hailey-Dunsheath, S., Nikola, T., Parshley, S. C., Stacey, G. J., Benford, D. J., & Staguhn, J. G. 2010, *ApJ*, 714, L147
- Ferland, G. J., et al., 2013, *RMXAA*, 49, 137
- Fioc M., & Rocca-Volmerange, B. 1997, *A&A*, 326, 950
- Hirashita, H., Buat, V., & Inoue, A. K. 2003, *A&A*, 410, 83
- Inoue, A. K., Hirashita, H., & Kamaya, H. 2000, *PASJ*, 52, 539
- Inoue, A. K., Hirashita, H., & Kamaya, H. 2001, *ApJ*, 555, 613
- Inoue, A. K. 2001, *AJ*, 122, 1788
- Inoue, A. K. 2011, *MNRAS*, 415, 2920
- Kaneker, N., Wagg, J., Ram Chary, R., & Carilli, C. 2013, *ApJ*, 771, L20

- Kawada, M., et al., 2011, PASJ, 63, 903
- Kennicutt, R. C., 1998, ARA&A, 36, 189
- Komatsu E., et al., 2011, ApJS, 192, 18
- Leitherer, C., et al., 1999, ApJS, 123, 3
- Madden, S. C., et al., 2012, IAU Symposium, 284, 141
- Madden, S. C., et al., 2013, PASP, 125, 600
- Maiolino, R., et al., 2005, A&A, 440, L51
- Matsuo, H., Arai, T., Nitta, T., & Kosaka, A. 2009, ASP Conference Series, 418, 451
- Mizutani, M., Onaka, T., & Shibai, H. 2002, A&A, 382, 610
- Nagao, T., Maiolino, R., Marconi, A., & Matsuhara, H. 2011, A&A, 526, A149
- Oesch, P. A., et al., 2013, arXiv:1309.2280
- Okamoto T., Nemmen R. S., & Bower R. G. 2008, MNRAS, 385, 161
- Okamoto T., & Frenk C. S. 2009, MNRAS, 399, L174
- Okamoto T., Frenk, C. S., Jenkins, A., & Theuns, T. 2010, MNRAS, 406, 208
- Oke, J. B. 1990, AJ, 99, 1621
- Ouchi, M., et al., 2013, ApJ, submitted (arXiv:1306.3572)
- Pettini, M., Kellogg, M., Steidel, C. C., Dickinson, M., Adelberger, K. L., & Giavalisco, M.
1998, ApJ, 508, 539
- Pirzkal, N., Rothberg, B., Ryan, R., Coe, D., Malhotra, S., Rhoads, J., & Noeske, K. 2013,
ApJ, in press (arXiv:1304.4594)

Schaerer, D. 2002, *A&A*, 382, 28

Schenker, M. A., et al., 2013, *ApJ*, 768, 196

Shimizu I., Inoue, A. K., Okamoto T., & Yoshida, N. 2013, *MNRAS*, submitted
(arXiv:1310.0114)

Springel, V., White, S. D. M., Tormen, G., Kauffmann, G., 2001, *MNRAS*, 328, 726

Springel V. 2005, *MNRAS*, 364, 1105

Tremonti, C. A., et al., 2004, *ApJ*, 613, 989

Trenti, M., et al., 2011, *ApJ*, 727, L39

Treu, T., Schmidt, K. B., Trenti, M., Bradley, L. D., & Stiavelli, M. 2013, *ApJ*, accepted
(arXiv:1308.5985)

van den Bergh, S., 2000, *The Galaxies of the Local Group*, Cambridge University Press

Walter, F., et al., 2012, *ApJ*, 752, 93

Ward, D. B., Dennison, B., Gull, G., & Harwit, M. 1975, *ApJ*, 202, L31

Zheng, W., et al., 2012, *Nature*, 489, 406